MINERALOGY OF CARBON-ENRICHED ROCKY EXTRA-SOLAR PLANETS FROM LABORATORY EXPERIMENTS.

K. Hakim[1,2], W. van Westrenen[2] and C. Dominik[1], [1]Anton Pannekoek Institute for Astronomy, University of Amsterdam, Science Park 904, 1098XH Amsterdam, The Netherlands (hakim.kaustubh@gmail.com), [2]Department of Earth Sciences, Vrije Universiteit Amsterdam, De Boelelaan 1085, 1081HV Amsterdam, The Netherlands.

Introduction: Studies on the occurrence rates of rocky extra-solar (exo) planets show that almost every star in our galaxy acts as a host to a rocky exoplanet [1]. Spectroscopic observations of newly born stars with high C/O ratios indicate the likely formation of carbon-enriched rocky exoplanets having several 100 times the amount of carbon than the relatively carbon-poor rocky planets in our solar system [2,3]. Several studies have investigated the mineralogy of carbon-poor planets [4-6], but although the composition of planetary cores in the Fe-S-C system [7] and phase relations in the Fe-Mg-Si-C-O system [8] have been explored experimentally, the mineralogical make up of carbon-enriched exoplanets remains poorly constrained.

Experimental methods: We prepared two types of bulk chemical compositions enriched in carbon in the Fe-Ca-Mg-Al-Si-C-S-O (FCMAS+CSO) system, C-deficient (1:0.06:1.2:0.08:1.2:0:0.28:4) and C-enriched (1:0.06:1:0.12:1:1.4:0.16:4), based on recent chemical modeling of condensates in protoplanetary disks [3]. We used an end-loaded piston cylinder apparatus to perform high-pressure high-temperature laboratory experiments on these compositional mixtures in graphite-platinum double capsules at pressures of 1-2 GPa and temperatures between 1250-1550 ºC. Though the C-deficient mixture does not contain carbon, carbon is provided to the run products by the graphite capsule during the experiment. Minerals and melt phases in our experimental run products were analyzed using energy- and wavelength-dispersive spectroscopy on an Electron Microprobe (EMPA) at the National Geological Facility, Utrecht University, Netherlands.

Results and Discussion:

Phase assemblages. As shown in Fig. 1, our run products typically contain a clear segregation into silicate and iron-rich phases. *P-T* phase diagrams of the two types of run products, C-deficient and C-enriched, are given in Fig. 2. In the C-deficient system, upon cooling orthopyroxene is formed first and clinopyroxene is formed at the lowest temperature while olivine is ubiquitously present and silicate melt disappears at lower temperatures. Two-liquid immiscibility with S-rich and S-poor Fe melts in iron-rich phases is observed in all C-deficient run products except the one at the lowest temperature. In the C-enriched system, graphite is present as dispersed grains in all runs. Olivine is present in all runs and silicate melt disappears at the lowest temperature. Spinel and clinopyroxene are found at lower temperatures, however no orthopyroxene is observed. A single S-rich Fe melt is present in all C-enriched runs.

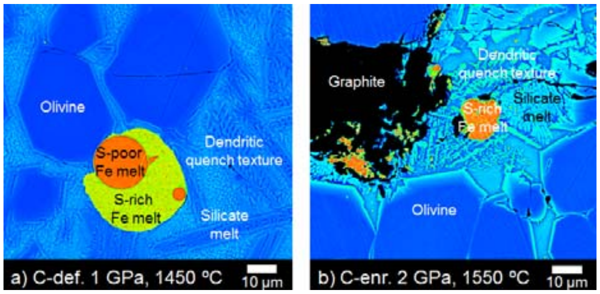

Fig. 1: *False-color backscattered electron images of typical C-deficient (a) and C-enriched (b) run products.*

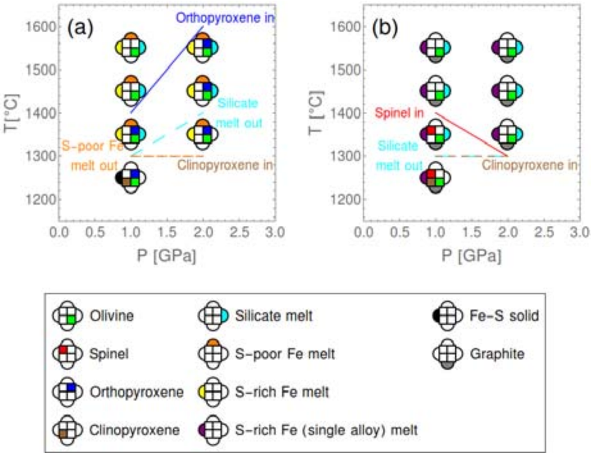

Fig. 2: *Phase diagrams of (a) C-deficient, and (b) C-enriched run products.*

Phase compositions. Pure graphite is observed in all C-enriched run products. Olivine is observed in both types of run products, however the Forsterite number of olivine in C-deficient runs is between 75-85 as opposed to C-enriched runs where it is between 55-75. Similar trend for Mg concentration is observed in pyroxenes and silicate melt. Most of Ca and Al are locked up in silicate melt and pyroxenes. On average, silicate melts of C-deficient and C-enriched runs contain 0.65 ± 0.14 wt% and 0.35 ± 0.04 wt% S^{2-}, respectively. Our initial estimates of the carbon concentrations in silicate melts of C-deficient and C-enriched runs, based on EMPA totals, are 0.3 wt% and 1.6 wt%, respectively. The volatile elements C and S are soluble in silicate melt and their solubility seems to be mutually exclusive. In C-deficient runs where the two-liquid immiscibility is observed in iron-rich melts, S-rich Fe melt contains an estimated ~1 wt% C with S/Fe ~ 1 and S-poor Fe melt contains an estimated ~5 wt% C with S/Fe ~ 0.03. In C-enriched runs, single S-rich Fe melt contains ~5 wt% C with S/Fe ~ 1. We do not observe immiscibility in the iron-rich melt of C-enriched runs likely because of different starting bulk S/Fe compositions in C-deficient and C-enriched mixtures.

Carbon-saturation in high-pressure experiments. Both C-deficient and C-enriched experiments were performed in graphite capsules, however the addition of 8.4 wt% C as graphite grains in the starting composition of C-enriched runs appears to increase the solubility of carbon in silicate melts. Previous studies [e.g., 9] assume graphite capsules to be sufficient to achieve carbon saturation. However, our experiments show that carbon-saturation may be best achieved by disseminating graphite grains throughout the sample.

Mineralogy of carbon-enriched rocky exoplanets. Our C-deficient and C-enriched experiments simulate conditions richer in carbon than those of the carbon-poor planets such as Earth and Mars. If a carbon-enriched rocky exoplanet contains significant amounts of carbon, most of the carbon will be present as graphite. Since graphite is lighter than the silicate minerals, it will likely be a part of its crust and upper mantle for a differentiated rocky exoplanet. If the graphite layers are deep enough, diamond layers could exist beneath them because of the high-pressure phase transition of graphite. The mantles of carbon-enriched rocky exoplanets may contain a variety of silicate minerals not much different from Earth and Mars such as olivine, pyroxenes, spinel and others depending on Mg/Si, Fe/Si ratios and Ca and Al abundances. Deeper in their mantles, perovskites and periclase can also be expected due to high-pressure phase transformations. Similar to a previous study [8], we did not observe carbonates implying it is probably difficult to form carbonates at large-scale in C-enriched planets. The absence of silicon carbide in our experiments combined with its presence in a previous study only at unrealistically reducing conditions indicates that silicon carbide is not stable in the interiors of carbon-enriched rocky exoplanets. The cores of carbon-enriched rocky exoplanets might show core stratification due to liquid immiscibility in the Fe-S-C system depending on S/Fe ratio and pressure conditions. Highly reduced Fe-rich cores may also contain Si in addition to S and C. Colder cores might contain solids like FeS, Fe-Si, Fe_3C and Fe_7C_3 depending on the right *P-T-X* conditions.

Effect of graphite on the mass of Kepler-102b. Due to graphite's lower density than silicate and iron-rich minerals, the mass of an exoplanet in the presence of significant amounts of graphite could be lower than expected for a given radius. To assess the effect of graphite on a planet's mass, we compute the interior structure of the recently discovered Mars-size exoplanet, Kepler-102b [10] by following the isothermal recipe to solve the hydrostatic and Poisson's gravitational gradient equations and keeping the radius fixed [11]. Assuming a fully differentiated interior of Kepler-102b with a pure iron core and an enstatite mantle and a fixed core/mantle mass ratio of 0.5, we find its total mass to be 0.75 times the Martian mass (0.75 M♂). When a 10 wt% graphite crust is added on the top of its mantle, its mass decreases by 8%. Moreover, the pressures at the bottom of graphite layers are high enough to form diamond layers. Carbon in the form of graphite can significantly alter the mass of an exoplanet for a fixed radius, a difference detectable by future space missions focusing on determinations of both mass and radius of rocky exoplanets.

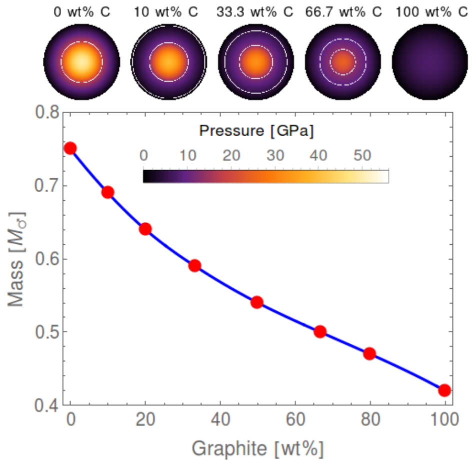

Fig. 3: *Red disks represent the total mass of Kepler-102b assuming an iron core, an enstatite mantle and a graphite crust with a core/mantle mass ratio of 0.5 and different mass fractions of graphite for a fixed planet's radius of 0.47 R♂ [10]. The internal pressure distribution of Kepler-102b is also shown for five cases where white contours represent the core-mantle and mantle-crust boundaries.*

References: [1] Burke C. J. et al. (2015) *ApJ, 809,* 8. [2] Bond J. C. et al. (2010) *ApJ, 715,* 1050-1070. [3] Moriarty J. et al. (2014) *ApJ, 787,* 81. [4] Stagno V. et al. (2013) *Nature, 493,* 84-88. [5] Vander Kaaden K. E. and McCubbin F. M. (2015) *JGR, 120,* 195-209. [6] Collinet M. et al. (2015) *EPSL, 427,* 83-94. [7] Dasgupta R. et al. (2009) *GCA, 73,* 6678-6691. [8] Takahashi S. et al. (2013) *PCM, 40,* 647-657. [9] Corgne A. et al. (2008) *GCA, 72,* 2409-2416. [10] Marcy G. W. et al. (2014) *ApJS, 210,* 20. [11] Unterborn C. T. et al. (2016) *ApJ, 819,* 32.